Free Radical Biology and Medicine 227 (2025) 582–592

Contents lists available at ScienceDirect

Free Radical Biology and Medicine

journal homepage: www.elsevier.com/locate/freeradbiomed

Static and dynamic *in vitro* colonic models reveal the spatiotemporal production of flavan-3-ol catabolites

Yongkai Ma [a], Lucia Ghiretti [b], Vincenzo Castellone [a], Pedro Mena [b,c], Josep Rubert [a,d,*]

[a] Food Quality and Design, Wageningen University & Research, Bornse Weilanden 9, Wageningen, 6708 WG, the Netherlands
[b] Human Nutrition Unit, Department of Food & Drug, University of Parma, Parma, Italy
[c] Microbiome Research Hub, University of Parma, Parma, Italy
[d] Division of Human Nutrition and Health, Wageningen University & Research, Stippeneng 4, Wageningen, 6708 WE, the Netherlands

ARTICLE INFO

Keywords:
Flavan-3-ols
Gut microbial metabolites
SHIME
Metabolomics
LC-MS
Gut microbiota

ABSTRACT

Flavan-3-ols are the most found flavonoid compounds in the human diet. Polymeric and monomeric flavan-3-ols reach the colonic region intact, where the gut microbiota utilizes them as substrates. In this research work, we investigated the pattern of colonic metabolites associated with flavan-3-ols, conducting a comprehensive analysis that combined (un)targeted metabolomics and *in vitro* colonic models. Firstly, the proposed flavan-3-ol metabolic pathway was investigated in-depth using a static *in vitro* model inoculated with different fecal donors. An apple, (−)-epicatechin, and procyanidin C1 were employed as feeding conditions. Small phenolic acids, such as phenylpropanoic acid and 3,4-dihydroxybenzoic acid, were positively associated with the apple feeding condition. In contrast, 5-(3',4'-dihydroxyphenyl)-γ-valerolactone and other specific early intermediates like phenylvaleric acids were positively associated with (−)-epicatechin. Secondly, by employing a dynamic *in vitro* simulator model of the human digestion system (SHIME), we reconstructed the flavan-3-ol metabolic pathway regionally. In the proximal colon region, we localized catabolites, such as 5-(3',4'-dihydroxyphenyl)-γ-valerolactone, while in the distal region, we identified mainly small phenolics. Combining static and dynamic *in vitro* models, we observed differences in the release of flavan-3-ol catabolites, influenced by both the food structure (isolated compounds and a food matrix) and the colonic region. This study sheds light on the colonic catabolism of one of the main dietary (poly)phenols and localizes microbial metabolites.

1. Introduction

Flavan-3-ols are widely present in many plant-based foods and beverages, such as cocoa, tea, wine, grapes, and stone fruits, and have been correlated with positive health outcomes, acting, for example, as immunomodulatory and anti-inflammatory compounds [1,2,3]. After digestion, most of the flavan-3-ols can reach the colon almost intact [4]. In this region, flavan-3-ols can either modulate microbial communities or undergo extensive microbial metabolism [5]. In the latter case, specific commensal bacteria utilize flavan-3-ols as substrate and release molecules with potential health benefits, such as phenyl-γ-valerolactones (PVLs), phenyl valeric acids (PVAs), and low molecular weight phenolics [1,6]. For instance, *in vitro*, we observed that chronic exposure to an epicatechin metabolite, (4R)-5-(3′,4′-dihydroxyphenyl)-γ-valerolactone, may lead to reduced colorectal cancer risk [7]. However, further studies are needed to localize this gut microbial metabolite (GMM) and determine whether this flavan-3-ol catabolite may protect against proximal, distal, or both regions.

The breakdown of flavan-3-ols begins with microorganisms biotransforming polymeric procyanidins in monomers mainly, followed by C-ring fission that forms small phenolics [1,3,6]. It is worth mentioning that the production of flavan-3-ol catabolites in humans depends on the type, quantity, and biological activity of the gut microbiota. During the last few years, researchers have explored the relationship between flavan-3-ols and donor-specific metabolism using fecal batch fermentation [8,9].Fecal batch fermentations lack regional information. Using a dynamic *in vitro* model, Li et al. addressed this issue and reported the region-dependent metabolic profiles of (+)-catechins, a type of flavan-3-ols, emphasizing the significance of intestinal regions and their associated microbial communities [5]. Therefore, it is important to investigate the differences in the formation of PVLs, PVAs, and phenolic acids, as well as their spatiotemporal production, since there has been

* Corresponding author. Food Quality and Design, Wageningen University & Research, Bornse Weilanden 9, Wageningen, 6708 WG, the Netherlands.
E-mail address: josep.rubert@wur.nl (J. Rubert).

https://doi.org/10.1016/j.freeradbiomed.2024.12.034
Received 17 June 2024; Received in revised form 3 December 2024; Accepted 12 December 2024
Available online 12 December 2024

little investigation into the spatiotemporal aspects of flavan-3-ols degradation [2,6,9–12]. Most of the abovementioned studies have employed pure standards to determine the catabolism of flavan-3-ols, and a few used food matrices rich in flavan-3-ols, such as a *Renetta Canada* apple [13]. In this study, we decided to compare pure isolated compounds and food matrices to decode the production and location of these flavan-3-ol catabolites.

The biotransformation of flavan-3-ols by commensal bacteria has been explored by different researchers using *in vitro* and *in vivo* approaches [6,10–16],. *In vivo* studies using humans and animals are crucial. *In vivo* models involve the use of living organisms, such as rodents, pigs, and human subjects, to investigate how dietary components affect the composition and function of the gut microbiota. However, there are limitations, such as interactions with other confounding variables, region-specific sampling in humans, ethical considerations, housing conditions, and differences in the gut microbiota composition in rodents, among others [17,18]. On the other hand, *in vitro* approaches are not exempt from limitations, such as lack of epithelial and immune compartments, absorption, differences between *in vitro* models, and challenges culturing strict anaerobic microorganisms [1,6,19–22]. Although they cannot replicate the full complexity of the human gastrointestinal tract, these models offer researchers a cost-effective and efficient way to explore hypotheses related to interactions between food and gut microbiota. So far, most of the studies have employed static *in vitro* models. A static *in vitro* model tends to mirror a specific region, adjusting the pH, and is stable for a short period [23]. As an alternative, dynamic *in vitro* models, such as the simulator of the human intestinal microbial ecosystem (SHIME). This powerful *in vitro* system enables long-term experimentation and significantly advances our knowledge of food-gut microbiota interactions, particularly in exploring spatiotemporal bio-transformations [16,24].

We suspect that the intestinal microenvironment impacts the biotransformation of flavan-3-ols. Thus, specific microbial communities in the proximal and distal colon may distinctly influence the catabolism of flavan-3-ols. However, the concrete spatiotemporal production of flavan-3-ol remains unclear. There is a valuable opportunity to further explore the spatiotemporal production of these metabolites along the colon, as this area has not yet been extensively researched. To overcome the current knowledge gap and localize the site of production of these key polyphenol catabolites, we first performed fecal batch cultures (FBC) to reconstruct the flavan-3-ol metabolic pathway. Secondly, the SHIME system determined the spatiotemporal production of GMMs. This study endeavored to explore the potential of combining static and dynamic *in vitro* models to reconstruct the breakdown of flavan-3-ols. By doing so, we aimed to delineate the spatiotemporal production of specific catabolites with relevant biological activities. Therefore, this new knowledge may contribute to the prevention of gastrointestinal diseases, such as colorectal cancer.

2. Materials and methods

2.1. Chemicals and reagents

Chemicals used in this study, including K_2HPO_4, KH_2PO_4, sodium thioglycolate, peptone, yeast extract, L-cysteine, tryptophan-d_5, *trans*-cinnamic-d_7, NaCl, $MgSO_4(H_20)_7$, $CaCl_2(H_20)_2$, Tween 80, bile salts, pepsin, pancreatin were acquired from Sigma-Aldrich (The Netherlands). Procyanidin C_1 (PC1) and 5-(3',4'-dihydroxyphenyl)-γ-valerolactone (DiHPVL) were purchased from Toronto Research Chemicals (Toronto, ON, Canada). Procyanidin B_2 (PB2), (−)-Epicatechin (EC), 3-(3',4'-dihydroxyphenyl)-propanoic acid (DiHPPA), 3',4'-dihydroxyphenylacetic acid (DiHPAA), 3,4-dihydroxybenzoic acid (DiHBA), 3-hydroxybenzoic acid (HBA), and benzoic acid (BA) were purchased from Sigma-Aldrich (St. Louis MO, USA). Apples, *Renetta Canada* variety, were purchased from a local shop in Trento (Italy). All chemicals and standards used in this study were LC-MS reagents unless otherwise stated. The nomenclature used for (poly)phenol catabolites follows the recommendations provided by Kay and co-authors [25].

2.2. Ethical consent

Wageningen University & Research's medical ethics committee assessed the study protocol and consent form and decided that this study does not require medical ethics approval (Registration Number 2023–16696). Participants signed an informed consent.

2.3. Fecal batch cultures (FBC): static model

Fecal samples were collected from four healthy participants (donors 1–4; two males and two females). Participants were advised to follow a flavanol-free diet for two weeks. They had an average age of 23 years, a body mass index between 20.0 and 23.9, and had not undergone any antibiotic treatment. Additionally, they had no history of gastrointestinal disorders for at least six months. Stool samples were collected at 9 a.m. and utilized within 2 h. FBC experiment protocol was performed as described by Pérez-Burillo et al. with a few modifications [16]. The pH value was adjusted to 6.6. All steps were carried out under sterile conditions. Firstly, 15 mg/L sodium thionate were added to 200 mL phosphate buffer. Then, 40 g fresh fecal samples were added and homogenized for 10 min, speed 300 rpm/min. After that, a 2 min centrifuge at 500 rpm was applied, and the supernatant was collected as the final fecal suspension. Secondly, 4.3 mL of an autoclaved basal nutrient medium was added to a sterilized penicillin bottle (volume 10 mL). Subsequently, for the flavan-3-ol treatment groups (EC and PC1), 2 mL of sterilized solution containing standards and 0.7 mL fecal suspension were added. The final concentration of EC and PC1 was 0.01 mg/mL. For the food matrix feeding condition, the total polyphenol content was reported previously [13]. *Renetta Canada* apple has a total polyphenol content of 276 mg/100 g, from which 206 mg/100 g were flavan-3-ols, as Koutsos and co-authors have reported [13]. The peel and pulp of *Renetta Canada* apple were digested following the INFOGEST protocol [26]. Two mL of a sterilized water solution containing 0.14 g of *Renetta Canada* apple, 0.7 mL of fecal suspension, and the basal medium were added to the flask (final volume 7 ml). Thus, the final concentration of flavan-3-ols in the flask was approximately 0.04 mg/ml. Blanks were filled up with sterilized water to have the same final volume as standards or apple samples. All flasks were flushed for 10 min with N_2/CO_2 to maintain the anaerobic condition. For each treatment and control, seven flasks were incubated at 37 °C with mild shaking (300 rpm), and 5 ml were collected for each time point (0, 2, 4, 6, 8, 24, and 48 h). All experiments were performed in duplicate. To stop enzymatic reactions, all samples were fast-frozen using liquid nitrogen at the appropriate time point and stored in the freezer (−20 °C) before extraction and analysis.

2.4. SHIME: dynamic model

Stools from donor 3 and donor 4 were inoculated in the SHIME (ProDigest, Belgium). The experimental design of SHIME and sampling was based on previous studies with minor modifications [27]. SHIME consists of two units that share a stomach and small intestine vessels. These units were then divided into two parallel Proximal Colon (PC) and two Distal Colon (DC) compartments. These compartments were inoculated with fresh fecal samples from donors 3 and 4. The pH was maintained at 5.6–5.9 for PC compartments and at 6.6–6.9 for DC compartments by adding 0.5 M HCL or NaOH. The SHIME system was kept at 37 °C using a warm water circulator (AC200, Thermo Fisher Scientific), mixed at 300 rpm using stirrers, and kept at anaerobic conditions by flushing N_2 daily for 10 min at 0.1 bar (~3–4L/min). After a two-week stabilization period [24,28], a two-week treatment began feeding every day at 8 a.m. with EC (0.01 mg/mL) and digested apple (0.14 g/mL intake) in the shared stomach and small intestine vessels.

This concentration of flavan-3-ols met the recommended nutrient intake per day for an adult as a total of 50 mg EC per donor intake during the treatment stage in the SHIME system [29]. During the EC and apple feeding period, samples were collected from PC and DC colon from donors 3 and 4 at 8:00 a.m., 14:00 p.m., and 18:00 p.m. every day. Lastly, a two-week washout period with flavan-3-ol-free medium was used to investigate the recovery of microbial communities after long-term treatment. During the washout stage period, samples were collected at 8:00 a.m. each day. All collected samples were immediately frozen using liquid nitrogen and stored (−20 °C). The volume of PC and DC compartments was kept constant at 250 and 400 mL, respectively.

2.5. Extraction methods

Slurries collected from FBC and SHIME were extracted according to Di Pede et al. [11] and Koutsos et al. [13] with minor modifications. Briefly, frozen samples were thawed and vortexed for 30s. Then, an aliquot of 0.5 mL was extracted using 0.5 mL of methanol/water (1:1) with 0.1 % formic acid using tryptophan-d_5 (2 mg/L) and *trans*-cinnamic-d_7 (2 mg/L) as internal standards. The samples were vortexed for 1 min and then subjected to ultrasonication at low temperature for 10 min. Samples were then transferred to the freezer (−20 °C) and stored for 1 h in darkness. Subsequently, they were centrifuged at 12000 rpm for 10 min at 4 °C, and then 0.2 mL supernatant was transferred into an LC-MS vial. Quality control (QC) pool samples were created for FBC and SHIME experiments to monitor untargeted metabolomics experiments. For each experiment, 0.02 mL of the individually extracted supernatants were pooled and vortexed for 30 s, and 0.2 mL of the mixture was transferred to LC-MS vials and employed as QC pools.

2.6. LC-QqQ analysis

PC1, EC, PB2, DiHPVL, DiHPPA, DiHPAA, DiHBA, HBA and BA were identified and quantified using a Shimadzu LCMS-8050 (Kyoto, Japan) following the method described by Liu et al. [9] with a few modifications. The UPLC unit consisted of an LC-20ADXR solvent delivery module, a DGU-20ASR degassing unit, a CTO-20AC column oven, an FCV-20AH2 valve unit, and a SIL-30AC autosampler. The mobile phase consisted of solvent A, water with 0.1 % formic acid, and solvent B with 0.1 % formic acid in acetonitrile using as analytical column an Acquity UPLC BEH C18 column 130 Å (1.7 μm, 2.1 mm × 100 mm, Waters, The Netherlands) connected to an Acquity UPLC BEH C18 Pre-column 130 Å (1.7 μm, 2.1 mm × 5 mm, Waters, The Netherlands). The autosampler temperature was set as 4 °C. The initial chromatographic conditions were set at 5 % B for 0.5 min, followed by a linear change to reach 35 % B at 2 min. Finally, 95 % B was achieved at 9.5 min prior to holding at 95 % for 1 min to allow for column washing before returning to initial conditions. Column reconditioning was completed in over 3 min, providing a total run time of 13.5 min. The injection value was 5 μL, the column was maintained at 40 °C, and a flow rate of 0.3 mL/min was used.

The triple quadrupole mass spectrometer was operated with an electrospray ionization source under the negative mode in the multiple reaction monitoring mode. ESI parameters were set as follows: nebulizing gas flow at 3.0 L/min; heating gas and drying gas flow at 10.0 L/min; desolations temperature at 250 °C; interface temperature at 300 °C and heat block temperature at 400 °C. Then metabolites were identified by comparing the retention times (RTs) and ion values of the samples with those of commercially available authentic standards: PC1 (*m/z* 865.1 → 125.0; RT 4.71 min), PB2 (*m/z* 577.1 → 407.1; RT 4.56 min), EC (*m/z* 289.1 → 245.0; RT 4.68 min), DiHPVL (*m/z* 207.1 → 163.0; RT 4.96 min), DiHPPA (*m/z* 181.2 → 136.9; RT 4.55 min), DiHPAA (*m/z* 167.3 → 123.0; RT 3.37 min), DiHBA (*m/z* 153.2 → 109.0; RT 2.54 min), HBA (*m/z* 137.2 → 92.9; RT 4.21 min), BA (*m/z* 121.0 → 77.0; RT 5.52 min). Finally, the data generated was acquired and analyzed using LabSolutions software (Shimadzu Corporation, Japan). The concentration range of the calibration curve concentration was 0.5–2000 ppb of standards in fecal slurries.

2.7. LC-QTOF analysis

Metabolites, such as 1-(3′,5′-dihydroxyphenyl)-3-(2′,4′,6′-trihydroxyphenyl)-propan-2-ol (DiHPP-2-ol), 1-(hydroxyphenyl)-3-(2′,4′,6′-trihydroxyphenyl)-propan-2-ol (HPP-2-ol), 4-hydroxy-5-(3′,4′-dihydroxy phenyl)valeric acid (4-H-DiHPVA), 5-(3′,4′-dihydroxyphenyl)valeric acid (DiHPVA), 5-(3′-hydroxyphenyl)-γ-valerolactone (HPVL), 5-(3′-hydroxyphenyl)valeric acid (HPVA), 3-(3-hydroxyphenyl)propanoic acid (HPPA), 3-hydroxyphenylacetic acid (HPAA), 5-phenylvaleric acid (PVA), phenylpropanoic acid (PPA), phenylacetic acid (PAA) were tentatively identified using a Nexera XS UPLC system (Shimadzu Corporation, Kyoto, Japan) coupled an LCMS-9030 quadrupole time-of-flight mass spectrometer (Shimadzu Corporation, Kyoto, Japan). The UPLC unit consisted of an LC-40D XS solvent delivery pump, a DGU-405 degassing unit, a CTO-40S column oven, a CBM-40 lite system controller, and a SIL-40CX3 autosampler. The LC-QTOF system was equipped with a standard electrospray ionization source unit (ESI) and a calibrant delivery system. The chromatographic separation was accomplished employing water (eluent A) and acetonitrile (eluent B), both acidified with 0.1 % formic acid, which were used as mobile phases. The gradient was as follows: start with 5 % B, linear increase to 95 % B in 8.5 min, for next 3.5 min was kept at 95 % B, switching to 5 % B in 12 min, and column equilibration for 2 min before the next injection. The flow rate was 0.3 mL/min and the oven temperature was kept at 40 °C. The injection volume was 5 μL. ESI source conditions: nebulizing gas flow, 2.0 L/min; heating gas flow 10.0 L/min; interface temperature 300 °C; desolations temperature 526 °C; interface voltage, 4.00 kV (positive) or 2.50 kV (negative); measurement *m/z*: 50–1000; the event time for the full scan was set at 0.1 s. MS data was collected with ion accumulation for 12 min. External mass calibration was performed by using ESI-L Low Concentration Tuning Mix 100 mL (Agilent Technologies, Amstelveen, The Netherlands). Both negative and positive ionization modes were used for the metabolomic analysis. The generated MS raw data (.lcd file) was processed using the MS-DIAL software (Version 4.9.221218) [30]. On the other hand, automatic peak screening using LabSolutions Insight Explore software (Shimadzu Corporation, Japan) was conducted with a local database that was created using flavan-3-ol metabolites. For identification, the MS tolerance for peak centroiding was set to 0.05 Da in LabSolutions Insight Explore software, and accurate mass tolerance was 0.01 Da for MS1 and 0.01 Da for MS2 in MS-DIAL software.

2.8. Short chain fatty acids (SCFAs) analysis

SCFAs, such as acetic acid, propionic acid, butyric acid, isobutyric acid, valeric acid and isovaleric acid were quantified using a Shimadzu GC-2014 (Kyoto, Japan) coupled with flame ionization detection (FID, Shimadzu, 's-Hertogenbosch, The Netherlands) following method as described in a previous reference with minor modification [31]. In short, 0.5 mL of slurry was taken and spun down at 9000 rpm for 5 min at 4 °C. Subsequently, 125 μL internal standard solution (0.45 mg/mL 2-ethylbutyric acid in 0.3M HCl and 0.9M oxalic acid) was added to 0.250 mL supernatant, vortexed 30 s and 0.150 mL mixture was transferred into a GC vial. The injection volume was 1 μL, and a Restek Stabilwax column (30 m × 0.25 mm × 0.25 μm, with a T Max of 240 °C, Restek, Santa Clara, CA, USA) was employed. Nitrogen served as carrier gas with a flow rate of 10 mL/min. Air, H_2, and N_2 were used as makeup gases at pressures of 260, 30, and 30 mL/min, respectively. The initial oven temperature was set at 100 °C, ramped up to 180 °C at 8 °C/min, then held for 1 min. Subsequently, the temperature increased to 200 °C at 50 °C/min and maintained at this level for 5 min. Finally, data generated was analyzed using Chromeleon 7.2 sr5® software (Thermo Scientific, Waltham, MA, USA).

2.9. Statistical analysis and software packages

In this study, all assays were performed with duplicates. Chem Draw 19.0 software (PerkinElmer, Waltham, USA) was used to draw metabolite structures. LC-QqQ analysis was conducted by the LabSolutions software (Shimadzu Corporation, Japan), while MS-Dial software (Version 4.9.221218) [30] for LC-QTOF-MS data. MetaboAnalyst5.0 (https://www.metaboanalyst.ca/) was employed to analyze multivariate empirical bayes analysis of variance (MEBA), analysis of variance (ANOVA), random forest, correlation analysis, enrichment and heatmaps of untargeted metabolomic data. MicrobeMASST (https://masst.gnps2.org/microbemasst/) was performed to link the metabolomics data to gut microbial producers [32].

3. Results and discussion

3.1. Biotransformation of flavan-3-ols: reconstructing the pathway using FBC

The first *in vitro* study aimed to investigate flavan-3-ol catabolites during 48h, collecting samples at 7-time points (Fig. S1). Flavan-3-ols and gut-related metabolites were quantified by LC-QqQ (Table S1), and those not commercially available were tentatively qualified using LC-QTOF (Table S1). In the latter, the identification criteria were based on (i) chromatographic separation, (ii) peak shape and resolution, (iii) the measured accurate mass of $[M + CH3COO]^-$, $[M-H]^-$ or $[M + HCOO]^-$ must fit the theoretical accurate mass with a mass tolerance set at ±5 ppm (Table S1), (iv) isotopic pattern, (v) fragment ions obtained, and (vi) references and databases [1,2,9].

3.2. (−)-Epicatechin

Previous studies have suggested diverse catabolic routes of flavan-3-ols [1,6,9–11]. These metabolic pathways may be modulated by the rate of conversion, time dependency, and, potentially, gut microbiota composition, highlighting interindividual differences [9]. Indeed, interindividual differences might be correlated with different enzymes, such as hydrolases, lyases, and oxidoreductases [33]. To enhance our understanding of the catabolic mechanism, we first examined the general biotransformation pathway (Fig. 1) by averaging all donors, and then explored the interindividual differences.

Regarding EC, we observed that the heterocyclic C-ring was cleaved at early time points to produce DiHPP-2-ol (Fig. 1), a result consistent with previous studies stating that C-ring opening is an initial metabolic step for EC biotransformation [2,9]. The *Ruminococcace* family has been positively correlated with the formation of DiHPP-2-ol and its downstream metabolites [9,34]. More specifically, the formation of DiHPP-2-ol is the result of C-ring reductive cleavage [35–37], a process that seems to be induced through the action of gut bacteria such as *Lactobacillus plantarum, Eggerthella lenta*, and *Flavonifractor plautii,* as mentioned in a previous study [38]. Our research is based on targeted and untargeted metabolomics data. Utilizing untargeted metabolomics data, we employed a taxonomically informed mass spectrometry tool called microbeMASST to connect metabolites with potential microbial composition [32]. Folling this strategy, *Eggerthella lenta,* and *Lactobacillus* were tentatively detected using microbeMASST [32] (Fig. S2). Subsequently, still in its early stages, DiHPP-2-ol was bio-transformed to DiHPVL or HPP-2-ol, respectively, through A-ring fission and oxidation. After that, more pronounced at time 24h, DiHPVL was converted to DiHPVA, HPVL, and other small phenolic acids through different degradation reactions, including de-lactonization, the reduction in the length of the aliphatic chain in PVA, and the dehydroxylation of the

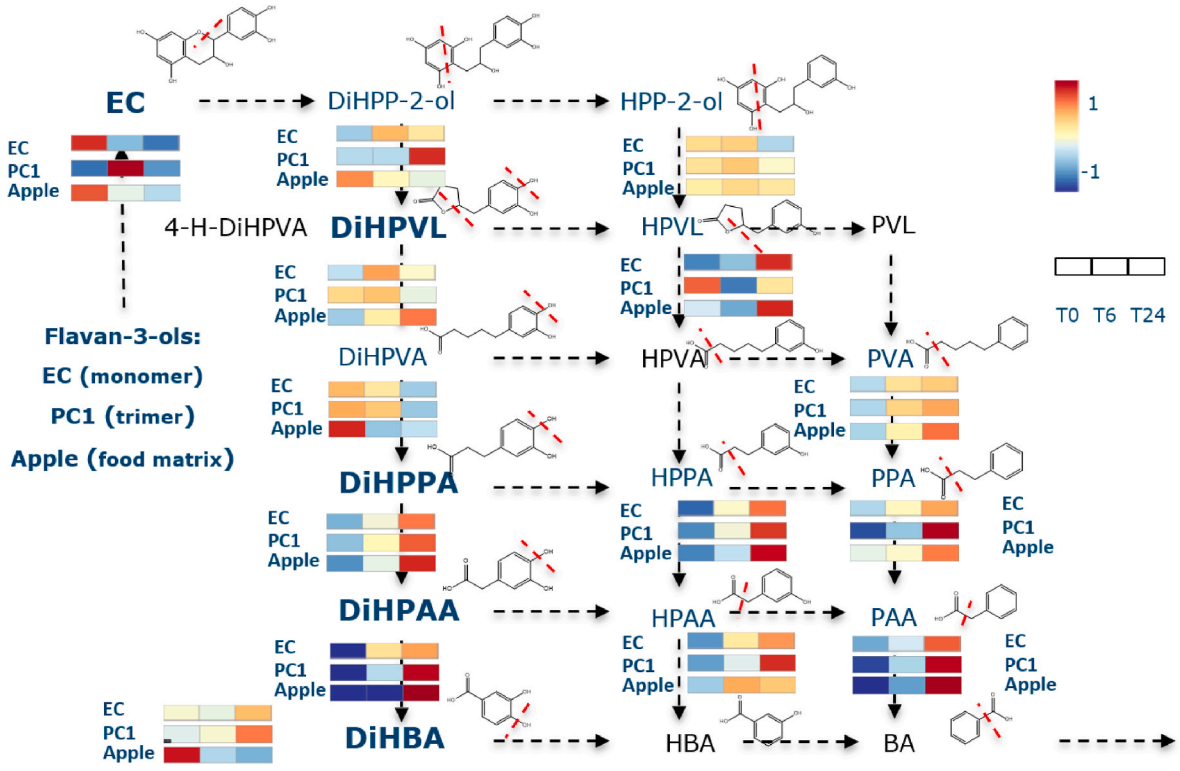

Fig. 1. Potential microbial pathway for EC, PC1, and apple using a static *in vitro* model. The names of the metabolites are represented in thin or bold characters, depending on whether they were detected by an LC-QTOF (qualitative data, thin) or LC-QqQ (quantitative data, **bold**). In the heatmap, a range from red (intense red, high levels) to blue (dark blue, low levels) represents the average relative intensity detected at 0, 6, and 24 h. (For interpretation of the references to color in this figure legend, the reader is referred to the Web version of this article.)

phenyl moiety [2,9]. Different microbes might be involved in these processes, among which *Phascolarctobacterium*, *Barnesiella*, *Akkermansia*, *Prevotella* and *Bacteroidota* [9]. HPVA, PVL, and BA were not detected during our fermentation batch cultures.

Our findings also revealed that metabolic profiles were donor-dependent (Fig. 2), which is consistent with the literature [8,9]. In line with this finding, Li et al., reported a type of flavan-3-ols, (+)-catechin also performed donor-dependent behavior *in vitro* [5]. We noticed EC was rapidly consumed by the gut microbiota (Fig. S3A), indicating GMMs started being released over time, as expected. However, we also observed temporal differences. Donors 1 and 2 showed different trends in producing DiHPVL from 0h to 48h (Fig. 2A). While donor 1 did not produce DiHPVL, donor 2 released increasing concentrations of this GMM from 4h to 48h. In addition, donors 3 and 4 behaved differently. Donor 4 can be defined as a fast converting since elevated levels of DiHPVL were produced between 2h and 48h. By contrast, Donor 3 started releasing DiHPVL after 24h. Thus, donor 3 could be considered a slow-converter of flavan-3-ols. Interestingly, after 48 h, DiHPVL was released at higher concentrations in Donor 3 compared to Donor 4. These differences between Donors 3 and 4 motivated us to select these donors for the subsequent SHIME experiments. At the microbial level, EC feeding conditions could have promoted the growth of the *Ruminococcace* family [9,34]. This might have beneficial implications for intestinal health since different species of *Ruminococcus*, particularly *R. bromii*, play a key role in breaking down fibers and starch.

3.3. Procyanidin C1

Microbial communities from the same donors were exposed to PC1, and LC-MS approaches were employed to characterize the flavan-3-ol catabolites (Fig. 1). During the initial stages (0–6 h), PC1 was mainly converted to EC in agreement with previous literature [11]. This trimer might be bio-transformed to a monomer through hydrolytic processes led by the *Lactobacillus* family [39,40]. After this initial metabolic step, the biotransformation followed the EC metabolic pathway. However, flavan-3-ol catabolites were produced later compared to EC feeding conditions (Fig. 1). By using isolated pure compounds, we observed that EC was bio-transformed more rapidly than PC1. However, we noticed that when PC1 was used as a feeding condition, HPVL concentrations dropped significantly ($p < 0.05$) at the 24-h sampling timepoint, confirming that this biotransformation step is affected by the degree of polymerization of flavan-3-ol.

A time-course quantitative assessment of PC1 catabolites is shown in Fig. 2A. This figure reveals a donor-dependent behavior similar to EC and indicates an interindividual variability consistent with the literature [2,6,9]. Overall, microbial communities metabolized PC1, leading to the formation of EC, DiHPVL, DiHPPA, DiHPAA, DiHBA, and HBA. As depicted in Fig. 2A, donors 3 and 4 presented different metabolic profiles characterized by different productions of DiHPVL and phenolic acids. DiHPVL was found at a higher level in donors 3 and 4, donor 3 being the main DiHPVL producer. In the end, the trend was opposite to EC feeding conditions. It indicates the different capacities of the gut microbiota on the biotransformation steps, from PC1 to EC and from EC to DiHPVL [1,9,11], showing that free flavan-3-ol and polymeric form affected the metabolic pathway (Fig. 2A).

3.4. Apple

An apple rich in flavan-3-ols was first digested following the INFOGEST protocol [26], and the undigested fraction was used to perform FBC. Fig. 1 indicates the most abundant metabolites derived from an apple. Note that apple's cell walls contain various microstructural elements, such as starch granules, proteins, and organelles, which have functional molecules [41]. The presence of these molecules might modulate microbial communities differently since we observed mainly PVL and other small catabolites (Fig. 1). In this sense, although the contribution of the catabolism of apple cinnamic derivatives to the production of some low molecular weight phenolic acids cannot be ruled

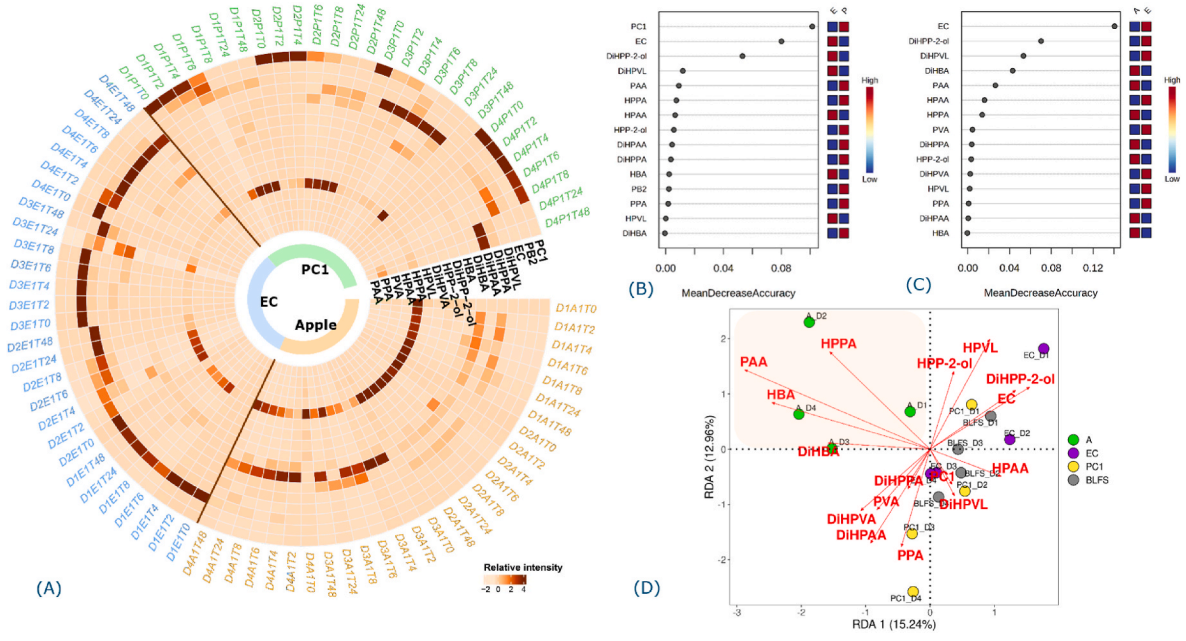

Fig. 2. (A) A heatmap of microbial metabolites was produced using longitudinal data, including 7-time points, 4 donors, and peak area information, from the static *in vitro* model with a range from −2 (light orange, low levels) to +4 (dark brown, high levels). A color-coded system depicts the feeding conditions; EC (blue), PC1 (green), and apple (orange). Random forest variable importance plots comparing (B) EC versus PC1 groups, and (C) EC versus apple were created. Longitudinal data, including all time points and peak area information, were uploaded to the online analysis platform of Metaboanalyst5.0 (https://www.metaboanalyst.ca/) to perform the random forest analysis. A higher value indicates the importance of the metabolite in predicting the group. (D) Redundancy analysis (RDA) analysis shows associations between flavan-3-ols catabolites and apple, EC, and PC1 feeding conditions at 24h (the control, thus, the basal medium inoculated with gut microbiota, is represented by the abbreviation BLFS). (For interpretation of the references to color in this figure legend, the reader is referred to the Web version of this article.)

out [42], the specificity of many compounds like PVLs and PVAs accounts for the robustness of this observation. This suggests that the food matrix may exert a higher contribution in regulating the bio-transformation of flavan-3-ol compared to the degree of polymerization of flavan-3-ols [13,43]. In addition, *Lactobacillus*, *Bifidobacterium,* and *Bacteroides* were computationally confirmed using MS data and microbeMASST (Fig. S2). This aligns with studies using rats as model organisms that were fed apple components [44–47].

By combining LC-QqQ and LC-QTOF data, we performed a random forest variable importance plot comparing EC and PC1 feeding conditions (Fig. 2B), as well as EC and apple feeding conditions (Fig. 2C). GMMs associated with flavan-3-ols potential microbial pathway (Fig. 1), including all sampling timepoint and peak area information, were selected and uploaded to the online analysis platform of Metaboanalyst5.0 (https://www.metaboanalyst.ca/) to perform the random forest analysis. The EC feeding group (Fig. 2B) had DiHPP-2-ol, DiHPVL, HPVL, and HPAA as main contributors. Statistical analyses revealed DiHPP-2-ol as a key intermediate in EC and PC1 groups using linear model, MEBA, and ANOVA analysis (Table S2). By contrast, when comparing EC and apple feeding conditions, DiHPP-2-ol, DiHPVL, HPVL, DiHPAA, HPVL, HPPA, PAA, DiHBA, and HBA were the most significant (Table S2), being small phenolics, the most significant in apple. To examine the interrelationships between different sets of variables, we employed a redundancy analysis (RDA) (Fig. 2D). As shown in

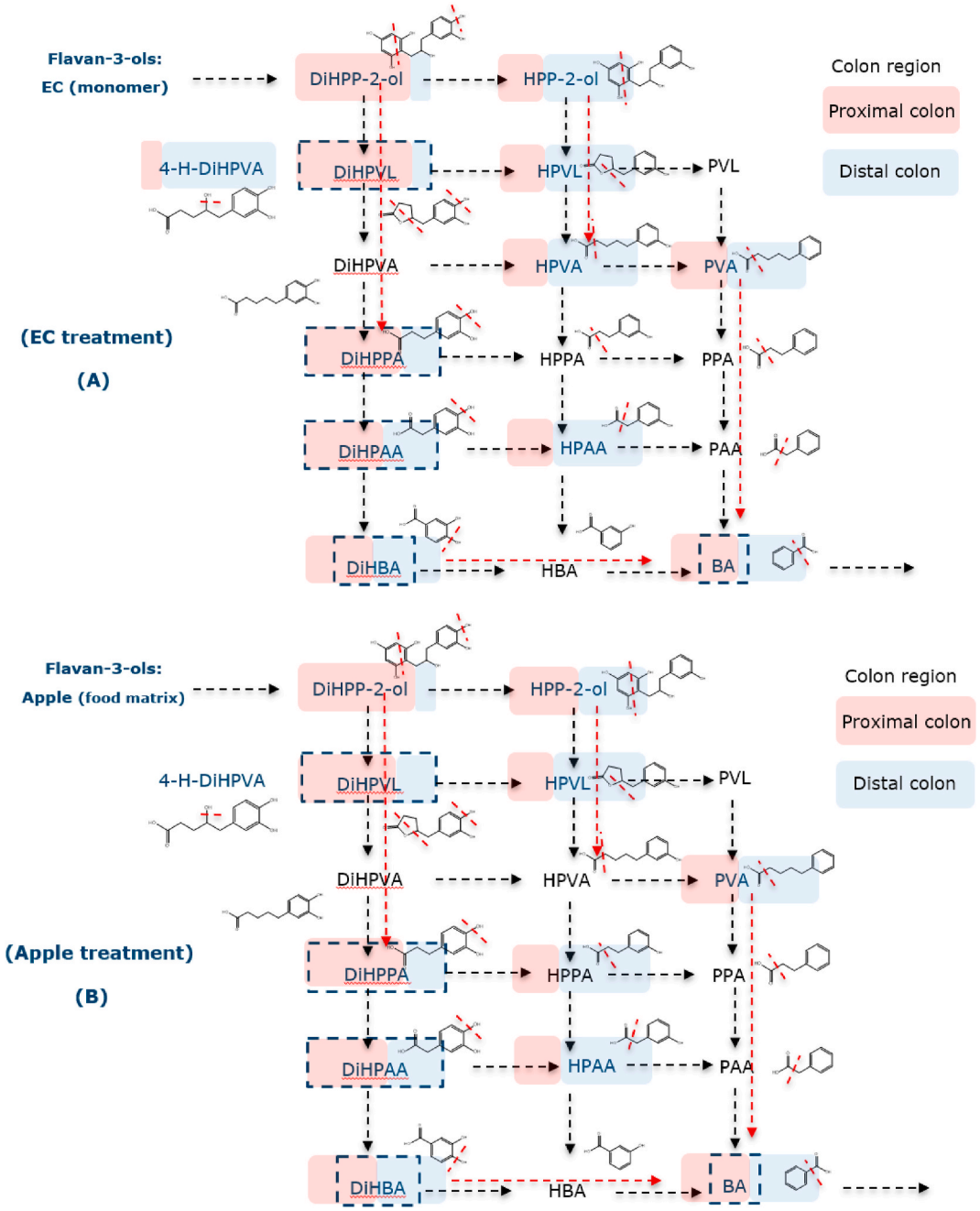

Fig. 3. Potential microbial metabolism pathway for EC (A) and apple (B) conditions reconstructed with the SHIME system. Metabolites whose text is colored in blue and with a dash line box were detected by LC-QqQ, and metabolites whose text is colored in blue were detected using LC-QTOF. The color of the boxes indicates the region in which the metabolite was generated: red box for PC, blue box for DC. More specifically, during the treatment period, for the metabolites that were detected in both PC and DC, the (relative) detection intensity is represented through the area occupied by the color in the box of the metabolite itself. (For interpretation of the references to color in this figure legend, the reader is referred to the Web version of this article.)

Fig. 2D, PAA, HPPA, DiHBA, and HBA were positively associated with the apple feeding condition. In other words, the end products of the underlined metabolic pathway were associated with the apple feeding condition. By contrast, the first intermediates, DiHPP-2-ol, HPP-2-ol, and HPVL, were positively associated with EC.

3.5. Biotransformation of flavan-3-ols: localizing flavan-3-ol catabolites in the SHIME

3.5.1. (−)-Epicatechin

By employing the SHIME system, we reconstructed the metabolic pathway of EC, comparing regional information and feeding conditions (Fig. 3A and B). At first glance, when comparing SHIME and FBC systems, we observed that HPVA, 4-H-DiHPVA, and BA were found in the SHIME system (Fig. 3A and B), while DiHPVA, HPPA, PPA, and PAA were mainly detected in FBC (Fig. 1). It indicates differences between *in vitro* models and specialized microbial communities from PC and DC [6, 10]. In the SHIME, differences between PC and DC regions at oxygen and pH levels might modulate microbial composition and function regionally. Indeed, a previous study demonstrated that the distal community had a higher relative abundance of *Finegoldia, Murdochiella, Peptoniphilus, Porphyromonas*, and *Anaerococcus*, and the proximal community had *Enterobacteriaceae, Bacteroidaceae*, and *Pseudomonas* [48].

EC was not detected in the DC of donors 3 and 4 during the first 24 h. Still, it was detected on the PC (Fig. S4). After 24 h of exposure, EC was detected in PC during the treatment stage (days 1–14), while the amount of EC rapidly decreased in the washout stage (days 15–28) (Fig. S4). This is in line with the FBC results where donor 4 was considered a fast-converter of flavan-3-ols. Consistent with this finding, Li and co-authors also reported a type of flavan-3-ol, (+)-catechin, had a donor-dependent converter efficiency (Q. [5]). In the PC region, EC breakdown metabolites, such as DiHPP-2-ol, 4-H-DiHPVA, DiHPVL, and HPP-2-ol, were produced at the early stages of the treatment stage (Fig. 4). By contrast, metabolites produced by shortening the aliphatic chain of phenyl-valeric acids were produced later. This is consistent with the FBC study and recent research works [2,6,9]. Interestingly, during the treatment period (days 1–7), the relation between 4-H-DiHPVA and DiHPVL in PC showed an opposite trend between donor 3 and donor 4 (Fig. 4), highlighting that this conversion step differed between donors. Overall, 4-H-DiHPVA was found at higher abundances in the DC when EC was used as a feeding condition (Fig. 4). Subsequently, DiHPPA was released in both the PC and DC regions. In PC, microbial communities from donors 3 and 4 highlighted similar behavior. However, in DC, donor 4 was more efficient in releasing flavan-3-ol catabolites.

When comparing PC and DC, we noticed that metabolites derived from DiHPP-2-ol were at higher abundances in PC, such as DiHPVL, indicating they might be PC metabolites. We investigated the concentration of DiHPVL in the PC of donor 4 (Fig. 4), which was higher

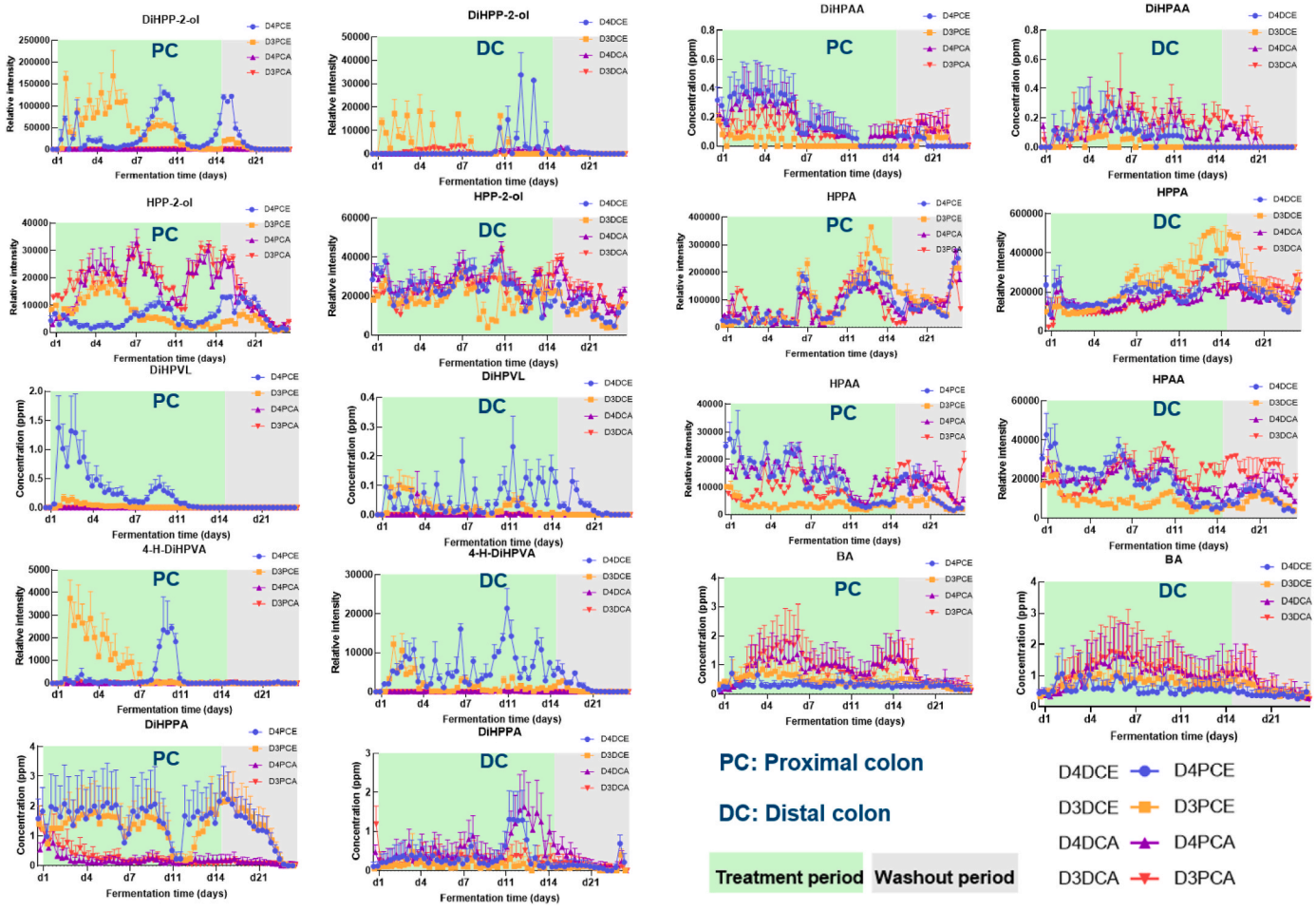

Fig. 4. Flavan-3-ol metabolites were semi-quantified and quantified during long-term experimental fermentation using epicatechin (EC) and apple feeding conditions. Treatment period (green background) and washout period (grey background). Data are presented as mean + SEM in each sampling time point during the SHIME period. Abbreviations: D4PCE stands for PC fed with EC (Donor 4); D3PCE represents PC fed with EC (Donor 3); D4PCA means PC fed with apple (Donor 4); D3PCA stands for PC fed with apple (Donor 3); D4DCE shows DC fed with EC (Donor 4); D3DCE highlights DC fed with EC (Donor 3); D4DCA represents DC fed with apple (Donor 4); and D3DCA, shows DC fed with apple (Donor 3). (For interpretation of the references to color in this figure legend, the reader is referred to the Web version of this article.)

compared to donor 3. This result agreed with the FBC result (Fig. 2A), indicating that the function of microbial communities was consistent between *in vitro* models. Although DiHPVL concentrations were low in the DC, donor 4 was able to produce more DiHPVL compared to donor 3.

Several metabolites, such as DiHPPA, DiHPAA, HPPA, HPAA, and BA, showed similar patterns (Fig. 4). However, we also observed inter-individual differences at early stages that were attenuated over time. For instance, DiHPP-2-ol, DiHPVL, 4-H-DiHPVA, and HPP-2-ol, had similar trends after 10 days of exposure to EC, indicating that chronic exposure to flavan-3-ols might modulate microbial communities to release a similar pattern of metabolites. The recovery of gut microbiota was investigated during the washout stage in both PC and DC regions, and we noticed that as soon as flavan-3-ols were not supplied, the production of flavan-3-ol specific catabolites dropped rapidly, while others, like HPPA and HPAA, diminished gradually over time.

3.6. Apple

The metabolic pathway of flavan-3-ols using the undigested fraction of an apple as a feeding condition was regionally reconstructed (Fig. 3B). When comparing SHIME and FBC systems, we observed that DiHPVA, PPA, and PAA were released in the FBC system (Fig. 1). By contrast, BA was mainly detected in SHIME (Fig. 3B). This is also in line with the EC feeding condition results (Fig. 3A).

On the other hand, when comparing apple and EC feeding conditions, we observed that 4-H-DiHPVA and HPVA were released when EC treatment was employed (Fig. 3A). In contrast, HPAA was mainly detected when the apple feeding condition was supplied (Fig. 3B). The pattern of flavan-3-ol catabolites significantly differed between EC and apple feeding conditions. Note that metabolites related to flavan-3-ol ring fission, such as DiHPVA and HPVL, were not detected when the apple treatment was supplied. Indeed, 4-H-DiHPVA, DiHPPA, and HPVA were only detected during EC treatment, indicating that EC cleavage could be regulated by the food matrix [1,13]. By contrast, the aliphatic chain of PVAs was shortened in both EC and apple feeding conditions (Fig. 4).

We also observed that metabolites like DiHPP-2-ol, HPP-2-ol, DiHPVL, and 4-H-DiHPVA behaved differently between the two feeding conditions (Fig. 4). Through the combination of LC-QqQ and LC-QTOF data, we performed Spearman correlation analysis comparing the peak areas of EC and apple feeding conditions in PC (Fig. S5A), as well as for EC and apple feeding conditions in DC (Fig. S5B). Flavan-3-ols catabolites, including all sampling timepoint and peak area information, were selected and uploaded to the online analysis platform of Metaboanalyst5.0 (https://www.metaboanalyst.ca/) to perform the Spearman correlation analysis. The Spearman correlation analysis confirmed positive correlations between DiHPP-2-ol, DiHPPA, DiHPVL, and 4-H-DiHPVA and EC feeding condition in PC (Fig. S5A). In contrast, HPP-2-ol, DiHPAA, DiHBA, HPAA, and BA were positively associated with apple feeding condition, which is in line with FBC results and also corresponds with previous literature [13]. We noticed that the production of DiHPP-2-ol and HPP-2-ol was matrix-dependent. DiHPP-2-ol was more abundant in EC feeding conditions, while HPP-2-ol was more abundant in the apple feeding condition. EC might be rapidly used by microbial communities, while the apple feeding condition contained both free and bound flavan-3-ols, which might be utilized differently.

When comparing PC and DC, we noticed that metabolites in DC were evenly produced no matter the feeding conditions (Table 2S). In contrast, the gut microbiota of PC seemed to be affected by the food matrix [24]. The relative abundances and concentrations of DiHPP-2-ol, DiHPVL, DiHPAA, PVA, and BA suggest that these metabolites were mainly produced in the PC. By contrast, HPP-2-ol, HPVL, DiHBA, and HPAA were mainly found in the DC region (Fig. 3B). Indeed, DiHPPA, HPP-2-ol, DiHPVL, HPAA, DiHBA, BA, 4-H-DiHPVA, DiHPAA, and PVL significantly differ between feeding conditions and colonic regions. This knowledge reveals new opportunities for flavan-3-ol interventions aimed at the gut epithelium. Releasing region-specific GMMs may help lower the risk of gastrointestinal diseases.

3.7. SCFAs result

SCFAs, not only play an important role in maintaining gut health but also reflect the status of gut microbiota [49]. So, in our study, we quantified SCFAs in PC and DC. As shown in Fig. 5, we observed that PC microbial communities exposed to EC did not vary the production of SCFAs compared to the baseline. However, the apple feeding condition modulated the production of SCFAs due to the presence of dietary fibers. After a fluctuation period of 4 days, SCFA levels remained steady, with the concentrations of acetic acid, propionic acid, and isobutyric acid higher than those of the EC feeding condition. In the DC, total SCFAs and individual SCFAs such as acetic acid, propionic acid, isobutyric acid, and valeric acid presented stable levels after 6 days of exposure to EC or apple feeding conditions, suggesting a longer period of adaptation of the gut microbiota. This finding reinforces the idea that gut microbiota is modulated by flavan-3-ols, not only affecting the breakdown of flavan-3-ols. In the end, the recovery of the gut microbiota was faster in the PC during the washout period, as was also observed for flavan-3-ol catabolites.

Furthermore, when comparing the production of SCFAs in PC and DC, we investigated differences between donors. For example, from day 1 to day 6, the production of SCFAs, such as acetic acid, butyric acid, isobutyric acid, and valeric acid behaved differently between Donor 3 and Donor 4. From day 7 to day 28, valeric acid exhibited donor dependence in the DC region, while total SCFA levels did not differ between donor 3 and donor 4, indicating that valeric acid producers may have different activities during this period. Both FBC and SHIME *in vitro* systems showed that the microbial metabolism of flavan-3-ols was donor-dependent. Consistent with this finding, Li et al. also reported that a type of flavan-3-ols, (+)-catechin, also exhibited donor-dependence [5]. Thus, the differences in composition and function of gut microbiota between PC and DC lead to varying production of SCFAs during their interaction with EC or apple, and further research is needed to clarify it [48].

3.8. Comparative analysis of metabolic pathways between FBC and SHIME experiments

Non-targeted metabolomics MS data acquired by an LC-QTOF, including FBC and SHIME data matrices, were analyzed to decipher metabolic pathways regulated during gut microbiota-flavan-3-ol interactions. After peak picking, alignment, normalization, and tentative identification, Hotelling-T2 values of the top 250 metabolites, which could map to KEGG pathways, were employed. Fig. 6 highlights the metabolic pathways regulated by the microbial communities (FBC, PC, and DC experiments). Notably, 13 metabolic pathways, such as purine metabolism, bile acid biosynthesis, thiamine metabolism, and riboflavin metabolism, among others, were shared by both FBC and SHIME systems. These results indicate that the microbial communities from FBC and SHIME exhibited consistent functionality. Fig. 6 also indicates that these metabolic pathways may play important roles in bio-transforming flavan-3-ols, influencing the production of metabolites. Moreover, it is acknowledged that microorganisms previously cited as potential actors in the transformation of the studied flavan-3-ols are also involved in some of these metabolic pathways. Different studies correlated the presence of *Firmicutes* with thiamine metabolism and betaine metabolism. In contrast, *Bacteroides* are positively correlated with thiamine, caffeine, and glutamate metabolism, and *Eggerthella lenta* seems to be involved in glutamate metabolism [50–56]. This might validate the hypothesis of the potential role of the cited microorganisms in the described metabolism. In line with this finding, *Eggerthella lenta* was confirmed using microbeMASST (Fig. S2).

Five metabolic pathways (Fig. 6A), like phosphatidylethanolamine

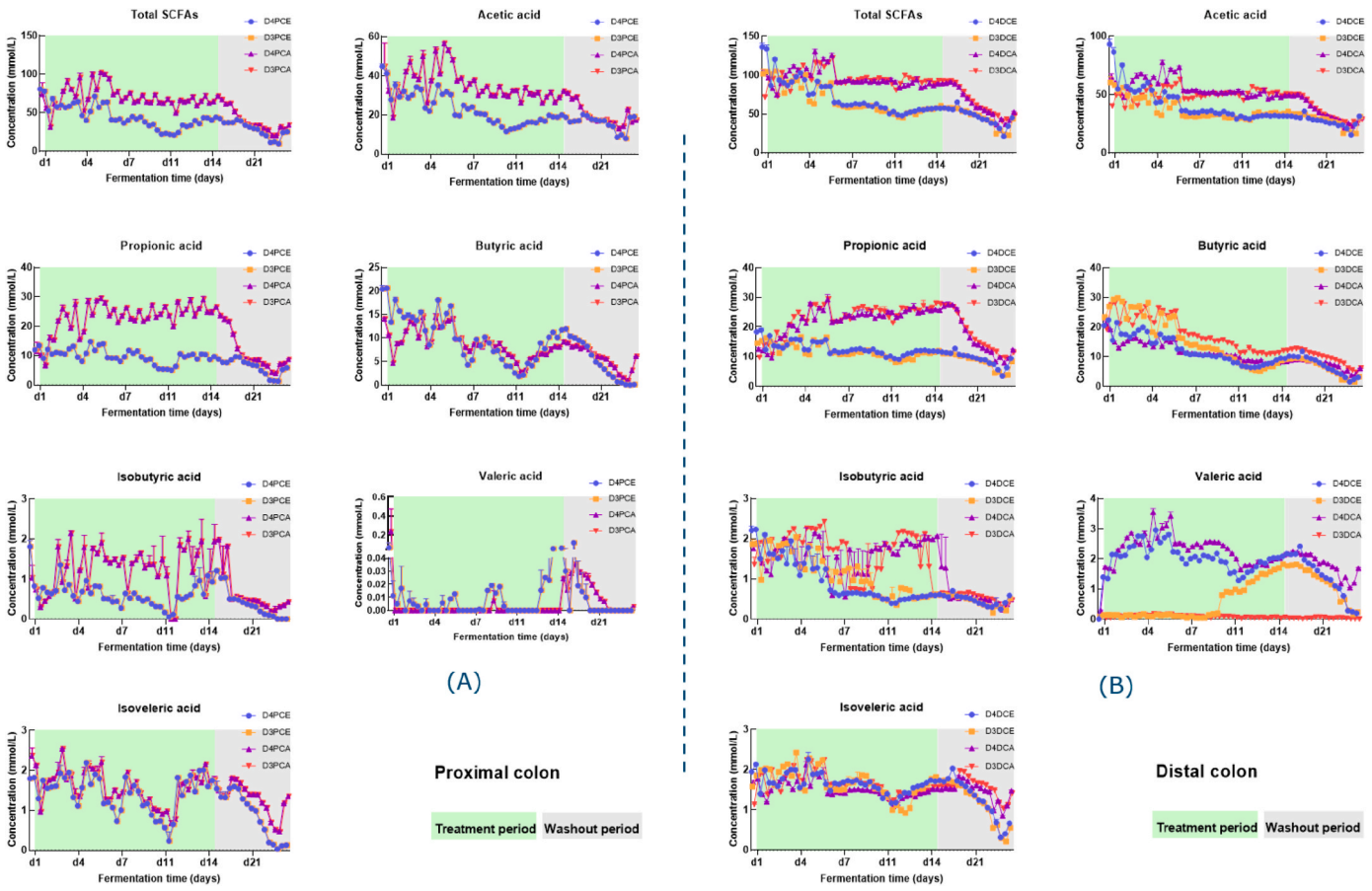

Fig. 5. Concentrations of total SCFAs, acetic acid, propionic acid, butyric acid, isobutyric acid, valeric acid, and isovaleric acid produced in the SHIME under EC and apple feeding conditions, including control (d0), treatment (d1-d14) and wash-out (d15-d28) period. (A) Proximal colon, (B) Distal colon. During the treatment period (green), EC or apple feeding conditions were used, while during the washout period (grey), a basic nutritional medium without feeding conditions was used. The data are presented as mean + SEM in each sampling time point during the SHIME period. Abbreviations: D4PCE stands for PC fed with EC (Donor 4); D3PCE represents PC fed with EC (Donor 3); D4PCA means PC fed with apple (Donor 4); D3PCA stands for PC fed with apple (Donor 3); D4DCE shows DC fed with EC (Donor 4); D3DCE highlights DC fed with EC (Donor 3); D4DCA represents DC fed with apple (Donor 4); and D3DCA, shows DC fed with apple (Donor 3). (For interpretation of the references to color in this figure legend, the reader is referred to the Web version of this article.)

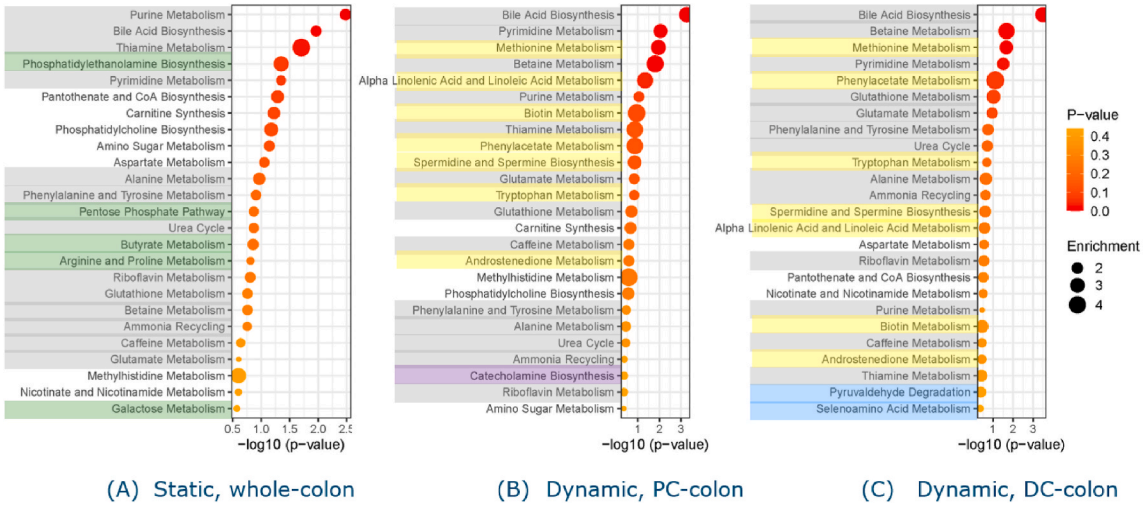

Fig. 6. Summary of metabolic pathways enrichment during the *in vitro* experiments using EC and apple feeding conditions. Firstly, the (A) static model was investigated in-depth, and secondly, the dynamic model was employed to determine differences between (B) proximal colon and (C) distal colon. Flavan-3-ol – gut microbiota interactions in static and dynamic conditions revealed common metabolic pathways (grey) and specific pathways for FBC (green), PC (purple), and DC (blue). The enrichment ratio represents the relative intensity of metabolites in the EC treatment divided by the apple feeding condition. (For interpretation of the references to color in this figure legend, the reader is referred to the Web version of this article.)

biosynthesis, pentose phosphate pathway, butyrate metabolism, arginine, proline metabolism, and galactose metabolism, only appeared to be relevant in FBC. On the other hand, catecholamine biosynthesis in the PC (Fig. 6B), pyruvaldehyde degradation, and selenoamino acid metabolism in the DC (Fig. 6C) were found such as methionine metabolism, alpha-linolenic acid, and linoleic acid metabolism, biotin metabolism, phenylacetate metabolism, spermidine and spermine biosynthesis, tryptophan metabolism, and androstenedione metabolism were mainly found in PC and DC, while not in FBC. It is tempting to speculate that the production of specific metabolites, like 4-H-DiHPVA and HPVA, might be regulated by gut microbes exerting these metabolic pathways and localized in specific regions. Therefore, 13 metabolic pathways might play a pivotal role in the catabolism of flavan-3-ols. Several pathways are differentially activated over time in the PC or DC regions. For example, 4-H-DiHPVA was generated with higher relative intensity under EC treatment in PC and DC regions, while it was not detected during short-term feeding conditions. This observation underlines the importance of complementing FBC studies with the SHIME, which localizes metabolites and permits the study of the mechanisms [2,57,58]. Our findings are also in line with recent research works, reporting that the gut microbiota not only can bio-transform flavan-3-ols but also modulate microbial communities [20,58,59]. To validate our findings, additional *in vitro* and *in vivo* studies examining enzyme activities and function of microbial communities are necessary.

4. Conclusions

In summary, we provided evidence of how flavan-3-ols are biotransformed and identified the site of their production using a combination of static and dynamic *in vitro* models. Initially, the static *in vitro* model, using EC, PC1, and a food matrix rich in flavan-3-ols, supported the reconstruction of the flavan-3-ol catabolic pathways. Although interindividual differences were observed, the first intermediates were mainly found when EC or PC1 were supplied. Secondly, flavan-3-ol catabolites were mapped in the SHIME system. Metabolites like 4-H-DiHPVA, HPVA, and BA were exclusively found in the dynamic *in vitro* system. In the PC, we localized metabolites related to EC ring fission, such as DiHPVL. In the DC, the most abundant catabolites were HPP-2-ol, HPVL, DiHBA, and HPAA. In this research, we have explained how flavan-3-ols, as single agents or present in a food matrix, could be utilized by microbial communities describing the spatiotemporal production of flavan-3-ol catabolites. In the long term, our research will offer new insights into the development of innovative probiotics aimed at enhancing the production of flavan-3-ol catabolites, along with strategies in food design and dietary interventions to prevent gastrointestinal diseases.

CRediT authorship contribution statement

Yongkai Ma: Writing – review & editing, Writing – original draft, Visualization, Methodology, Investigation, Formal analysis, Data curation. **Lucia Ghiretti:** Writing – review & editing, Writing – original draft, Visualization, Methodology, Investigation, Formal analysis, Data curation, Conceptualization. **Vincenzo Castellone:** Writing – review & editing, Methodology, Investigation, Formal analysis, Data curation. **Pedro Mena:** Writing – review & editing, Conceptualization. **Josep Rubert:** Writing – review & editing, Writing – original draft, Supervision, Software, Resources, Project administration, Methodology, Investigation, Funding acquisition, Formal analysis, Data curation, Conceptualization.

Declaration of interest

None.

Acknowledgments

The Food Quality and Design chair group at Wageningen University supported this research using internal funding. Yongkai Ma was supported by a China Scholarship Council [grant number 202106150104]. The authors express their gratitude to Dr. Christos Fryganas and Mr. Geert Meijer for their assistance with LC-MS and GC-FID analyses.

Appendix A. Supplementary data

Supplementary data to this article can be found online at https://doi.org/10.1016/j.freeradbiomed.2024.12.034.

References

[1] G. Di Pede, P. Mena, L. Bresciani, M. Achour, R.M. Lamuela-Raventós, R. Estruch, D. Del Rio, Revisiting the bioavailability of flavan-3-ols in humans: a systematic review and comprehensive data analysis, Mol. Aspect. Med. 89 (2023), https://doi.org/10.1016/j.mam.2022.101146. October 2022.
[2] G. Di Pede, P. Mena, L. Bresciani, T.M. Almutairi, D. Del Rio, M.N. Clifford, A. Crozier, Human colonic catabolism of dietary flavan-3-ol bioactives, Mol. Aspect. Med. 89 (May 2022) (2023) 101107, https://doi.org/10.1016/j.mam.2022.101107.
[3] Q. Xu, Q. Fu, Z. Li, H. Liu, Y. Wang, X. Lin, Y. Sun, The flavonoid procyanidin C1 has senotherapeutic activity and increases lifespan in mice, Nat. Metab. 3 (12) (2021) 1706–1726, https://doi.org/10.1038/s42255-021-00491-8.
[4] D. Carregosa, C. Pinto, M.Á. Ávila-Gálvez, P. Bastos, D. Berry, C.N. Santos, A look beyond dietary (poly)phenols: the low molecular weight phenolic metabolites and their concentrations in human circulation, Compr. Rev. Food Sci. Food Saf. 21 (5) (2022) 3931–3962, https://doi.org/10.1111/1541-4337.13006.
[5] Q. Li, J. Stautemas, S. Omondi Onyango, M. De Mey, D. Duchi, E. Tuenter, T. Van de Wiele, Human gut microbiota stratified by (+)-catechin metabolism dynamics reveals colon region-dependent metabolic profile, Food Chem. 408 (2023) 1–11, https://doi.org/10.1016/j.foodchem.2022.135203.
[6] P. Mena, L. Bresciani, N. Brindani, I.A. Ludwig, G. Pereira-Caro, D. Angelino, D. Del Rio, Phenyl-γ-valerolactones and phenylvaleric acids, the main colonic metabolites of flavan-3-ols: synthesis, analysis, bioavailability, and bioactivity, Nat. Prod. Rep. 36 (5) (2019) 714–752, https://doi.org/10.1039/c8np00062j.
[7] J. Rubert, P. Gatto, M. Pancher, V. Sidarovich, C. Curti, P. Mena, F. Mattivi, A screening of native (Poly)phenols and gut-related metabolites on 3D HCT116 spheroids reveals gut health benefits of a flavan-3-ol metabolite, Mol. Nutr. Food Res. 66 (21) (2022) 1–27, https://doi.org/10.1002/mnfr.202101043.
[8] J. Lessard-Lord, C. Roussel, V. Guay, Y. Desjardins, Characterization of the interindividual variability associated with the microbial metabolism of (−)-Epicatechin, J. Agric. Food Chem. 71 (37) (2023) 13814–13827, https://doi.org/10.1021/acs.jafc.3c05491.
[9] C. Liu, J. Vervoort, K. Beekmann, M. Baccaro, L. Kamelia, S. Wesseling, I.M.C. M. Rietjens, Interindividual differences in human intestinal microbial conversion of (-)-Epicatechin to bioactive phenolic compounds, J. Agric. Food Chem. 68 (48) (2020) 14168–14181, https://doi.org/10.1021/acs.jafc.0c05890.
[10] E.M. Campos, P. Stehle, M.C. Simon, Microbial metabolites of flavan-3-ols and their biological activity, Nutrients 11 (10) (2019) 1–27, https://doi.org/10.3390/nu11102260.
[11] G. Di Pede, L. Bresciani, F. Brighenti, M.N. Clifford, A. Crozier, D. Del Rio, P. Mena, In vitro faecal fermentation of monomeric and oligomeric flavan-3-ols: catabolic pathways and stoichiometry, Mol. Nutr. Food Res. 66 (21) (2022) 2101090, https://doi.org/10.1002/mnfr.202101090.
[12] S. Stoupi, G. Williamson, J.W. Drynan, D. Barron, M.N. Clifford, A comparison of the in vitro biotransformation of (-)-epicatechin and procyanidin B2 by human faecal microbiota, Mol. Nutr. Food Res. 54 (6) (2010) 747–759, https://doi.org/10.1002/mnfr.200900123.
[13] A. Koutsos, M. Lima, L. Conterno, M. Gasperotti, M. Bianchi, F. Fava, K.M. Tuohy, Effects of commercial apple varieties on human gut microbiota composition and metabolic output using an in vitro colonic model, Nutrients 9 (6) (2017) 1–23, https://doi.org/10.3390/nu9060533.
[14] A. Anesi, P. Mena, A. Bub, M. Ulaszewska, D. Del Rio, S.E. Kulling, F. Mattivi, Quantification of urinary phenyl-γ-valerolactones and related valeric acids in human urine on consumption of apples, Metabolites 9 (11) (2019), https://doi.org/10.3390/metabo9110254.
[15] Z. Liu, M.E. Bruins, L. Ni, J.P. Vincken, Green and black tea phenolics: bioavailability, transformation by colonic microbiota, and modulation of colonic microbiota, J. Agric. Food Chem. 66 (32) (2018) 8469–8477, https://doi.org/10.1021/acs.jafc.8b02233.
[16] S. Pérez-Burillo, S. Molino, B. Navajas-Porras, Á.J. Valverde-Moya, D. Hinojosa-Nogueira, A. López-Maldonado, J.Á. Rufián-Henares, An in vitro batch fermentation protocol for studying the contribution of food to gut microbiota composition and functionality, Nat. Protoc. 16 (7) (2021) 3186–3209, https://doi.org/10.1038/s41596-021-00537-x.
[17] F. Hugenholtz, W.M. de Vos, Mouse models for human intestinal microbiota research: a critical evaluation, Cell. Mol. Life Sci. 75 (1) (2018) 149–160, https://doi.org/10.1007/s00018-017-2693-8.

[18] D. Shalon, R.N. Culver, J.A. Grembi, J. Folz, P.V. Treit, H. Shi, K.C. Huang, Profiling the human intestinal environment under physiological conditions, in: Nature, vol. 617, Springer US, 2023, https://doi.org/10.1038/s41586-023-05989-7.
[19] C. Cueva, A. Jiménez-Girón, I. Muñoz-González, A. Esteban-Fernández, I. Gil-Sánchez, M. Dueñas, M.V. Moreno-Arribas, Application of a new Dynamic Gastrointestinal Simulator (SIMGI) to study the impact of red wine in colonic metabolism, Food Res. Int. 72 (2015) 149–159, https://doi.org/10.1016/j.foodres.2015.03.003.
[20] D. Ercolini, V. Fogliano, Food design to feed the human gut microbiota, J. Agric. Food Chem. 66 (15) (2018) 3754–3758, https://doi.org/10.1021/acs.jafc.8b00456.
[21] I. Gil-Sánchez, C. Cueva, M. Sanz-Buenhombre, A. Guadarrama, M.V. Moreno-Arribas, B. Bartolomé, Dynamic gastrointestinal digestion of grape pomace extracts: bioaccessible phenolic metabolites and impact on human gut microbiota, J. Food Compos. Anal. 68 (2018) 41–52, https://doi.org/10.1016/j.jfca.2017.05.005. May 2017.
[22] C.N. Spencer, J.L. McQuade, V. Gopalakrishnan, J.A. McCulloch, M. Vetizou, A. P. Cogdill, J.A. Wargo, Dietary fiber and probiotics influence the gut microbiome and melanoma immunotherapy response, Science 374 (6575) (2021) 1632–1640, https://doi.org/10.1126/science.aaz7015.
[23] L. Li, E. Abou-Samra, Z. Ning, X. Zhang, J. Mayne, J. Wang, D. Figeys, An in vitro model maintaining taxon-specific functional activities of the gut microbiome, Nat. Commun. 10 (1) (2019), https://doi.org/10.1038/s41467-019-12087-8.
[24] A.M. Rovalino-Córdova, V. Fogliano, E. Capuano, Effect of bean structure on microbiota utilization of plant nutrients: an in-vitro study using the simulator of the human intestinal microbial ecosystem (SHIME®), J. Funct.Foods 73 (March) (2020) 104087, https://doi.org/10.1016/j.jff.2020.104087.
[25] C.D. Kay, M.N. Clifford, P. Mena, G.J. McDougall, C. Andres-Lacueva, A. Cassidy, A. Crozier, Recommendations for standardizing nomenclature for dietary (poly) phenol catabolites, Am. J. Clin. Nutr. 112 (4) (2020) 1051–1068, https://doi.org/10.1093/ajcn/nqaa204.
[26] A. Brodkorb, L. Egger, M. Alminger, P. Alvito, R. Assunção, S. Ballance, I. Recio, INFOGEST static in vitro simulation of gastrointestinal food digestion, Nat. Protoc. 14 (4) (2019) 991–1014, https://doi.org/10.1038/s41596-018-0119-1.
[27] Z. Huang, J. Boekhorst, V. Fogliano, E. Capuano, J.M. Wells, Impact of high-fiber or high-protein diet on the capacity of human gut microbiota to produce tryptophan catabolites, J. Agric. Food Chem. 71 (18) (2023) 6956–6966, https://doi.org/10.1021/acs.jafc.2c08953.
[28] M. Marzorati, V. Maquet, S. Possemiers, Fate of chitin-glucan in the human gastrointestinal tract as studied in a dynamic gut simulator (SHIME®), J. Funct. Foods 30 (2017) 313–320, https://doi.org/10.1016/j.jff.2017.01.030.
[29] L. Gu, M.A. Kelm, J.F. Hammerstone, G. Beecher, J. Holden, D. Haytowitz, R. L. Prior, Concentrations of proanthocyanidins in common foods and estimations of normal consumption, J. Nutr. 134 (3) (2004) 613–617, https://doi.org/10.1093/jn/134.3.613.
[30] H. Tsugawa, T. Cajka, T. Kind, Y. Ma, B. Higgins, K. Ikeda, M. Arita, MS-DIAL: data-independent MS/MS deconvolution for comprehensive metabolome analysis, Nat. Methods 12 (6) (2015) 523–526, https://doi.org/10.1038/nmeth.3393.
[31] Z. Huang, T. Schoones, J.M. Wells, V. Fogliano, E. Capuano, Substrate-driven differences in tryptophan catabolism by gut microbiota and aryl hydrocarbon receptor activation, Mol. Nutr. Food Res. 65 (13) (2021) 1–9, https://doi.org/10.1002/mnfr.202100092.
[32] S. Zuffa, R. Schmid, A. Bauermeister, P.W. Paulo, A.M. Caraballo-Rodriguez, Y. El Abiead, P.C. Dorrestein, microbeMASST: a taxonomically informed mass spectrometry search tool for microbial metabolomics data, Nature Microbiology 9 (2) (2024) 336–345, https://doi.org/10.1038/s41564-023-01575-9.
[33] N. Koppel, V.M. Rekdal, E.P. Balskus, Chemical transformation of xenobiotics by the human gut microbiota, Science 356 (6344) (2017) 1246–1257, https://doi.org/10.1126/science.aag2770.
[34] K.F. Corral-Jara, S. Nuthikattu, J. Rutledge, A. Villablanca, R. Fong, C. Heiss, D. Milenkovic, Structurally related (−)-epicatechin metabolites and gut microbiota derived metabolites exert genomic modifications via VEGF signaling pathways in brain microvascular endothelial cells under lipotoxic conditions: integrated multi-omic study, J. Proteonomics 263 (2022) 104603, https://doi.org/10.1016/j.jprot.2022.104603.
[35] M. Glensk, W.J. Hurst, V.B. Glinski, M. Bednarski, J.A. Glinski, Isolation of 1-(30,40-Dihydroxyphenyl)-3-(2",4",6"-trihydroxyphenyl)-propan-2-ol from grape seed extract and evaluation of its antioxidant and antispasmodic potential, Molecules 24 (13) (2019), https://doi.org/10.3390/molecules24132466.
[36] F. Sánchez-Patán, R. Tabasco, M. Monagas, T. Requena, C. Peláez, M.V. Moreno-Arribas, B. Bartolomé, Capability of lactobacillus plantarum IFPL935 to catabolize flavan-3-ol compounds and complex phenolic extracts, J. Agric. Food Chem. 60 (29) (2012) 7142–7151, https://doi.org/10.1021/jf3006867.
[37] M.V. Selma, J.C. Espín, F.A. Tomás-Barberán, Interaction between phenolics and gut microbiota: role in human health, J. Agric. Food Chem. 57 (15) (2009) 6485–6501, https://doi.org/10.1021/jf902107d.
[38] M. Kutschera, W. Engst, M. Blaut, A. Braune, Isolation of catechin-converting human intestinal bacteria, J. Appl. Microbiol. 111 (1) (2011) 165–175, https://doi.org/10.1111/j.1365-2672.2011.05025.x.
[39] E. Dempsey, S.C. Corr, Lactobacillus spp. for gastrointestinal health: current and future perspectives, Front. Immunol. 13 (2022) 840245, https://doi.org/10.3389/fimmu.2022.840245.
[40] Z. Liu, W.J.C. De Bruijn, M.E. Bruins, J.P. Vincken, Microbial metabolism of theaflavin-3,3′-digallate and its gut microbiota composition modulatory effects, J. Agric. Food Chem. 69 (1) (2021) 232–245, https://doi.org/10.1021/acs.jafc.0c06622.
[41] J.M. Aguilera, The food matrix: implications in processing, nutrition and health, Crit. Rev. Food Sci. Nutr. 59 (22) (2019) 3612–3629, https://doi.org/10.1080/10408398.2018.1502743.
[42] G. Di Pede, P. Mena, L. Bresciani, M. Achour, R.M. Lamuela-Raventós, R. Estruch, D. Del Rio, A systematic review and comprehensive evaluation of human intervention studies to unravel the bioavailability of hydroxycinnamic acids, Antioxidants Redox Signal. 40 (7–9) (2024) 510–541, https://doi.org/10.1089/ars.2023.0254.
[43] E. Capuano, A.E.M. Janssen, Food matrix and macronutrient digestion, Annu. Rev. Food Sci. Technol. 12 (2021) 193–212, https://doi.org/10.1146/annurev-food-032519-051646.
[44] T. Jiang, X. Gao, C. Wu, F. Tian, Q. Lei, J. Bi, X. Wang, Apple-derived pectin modulates gut microbiota, improves gut barrier function, and attenuates metabolic endotoxemia in rats with diet-induced obesity, Nutrients 8 (3) (2016) 126, https://doi.org/10.3390/NU8030126.
[45] S. Masumoto, A. Terao, Y. Yamamoto, T. Mukai, T. Miura, T. Shoji, Non-absorbable apple procyanidins prevent obesity associated with gut microbial and metabolomic changes, Scientific Reports 2016 6 (1) (2016) 1–10, https://doi.org/10.1038/srep31208, 6(1).
[46] S. Sembries, G. Dongowski, G. Jacobasch, K. Mehrlä Nder, F. Will, H. Dietrich, H. Dietrich, Effects of dietary fibre-rich juice colloids from apple pomace extraction juices on intestinal fermentation products and microbiota in rats, Br. J. Nutr. 90 (3) (2003) 607–615, https://doi.org/10.1079/bjn2003925.
[47] S. Sembries, G. Dongowski, K. Mehrländer, F. Will, H. Dietrich, Physiological effects of extraction juices from apple, grape, and red beet pomaces in rats, J. Agric. Food Chem. 54 (26) (2006) 10269–10280, https://doi.org/10.1021/JF0618168.
[48] K.J. Flynn, M.T. Ruffin, D. Kim Turgeon, P.D. Schloss, Spatial variation of the native colon microbiota in healthy adults, Cancer Prev. Res. 11 (7) (2018) 393–401, https://doi.org/10.1158/1940-6207.CAPR-17-0370.
[49] B. Dalile, L. Van Oudenhove, B. Vervliet, K. Verbeke, The role of short-chain fatty acids in microbiota–gut–brain communication, Nat. Rev. Gastroenterol. Hepatol. 16 (8) (2019) 461–478, https://doi.org/10.1038/s41575-019-0157-3.
[50] Y. Fan, Y. Qin, M. Chen, X. Li, R. Wang, Z. Huang, C. Lu, Prenatal low-dose DEHP exposure induces metabolic adaptation and obesity: role of hepatic thiamine metabolism, J. Hazard Mater. 385 (2020) 121534, https://doi.org/10.1016/j.jhazmat.2019.121534.
[51] H. Jang, H. Lim, K. Park, S. Park, H. Lee, Changes in plasma choline and the betaine-to-choline ratio in response to 6-month lifestyle intervention are associated with the changes of lipid profiles and intestinal microbiota: the icaan study, Nutrients 13 (11) (2021), https://doi.org/10.3390/nu13114006.
[52] A. Nehlig, Effects of coffee on the gastro-intestinal tract: a narrative review and literature update, Nutrients 14 (2) (2022), https://doi.org/10.3390/nu14020399.
[53] P. Sittipo, J. Choi, S. Lee, Y.K. Lee, The function of gut microbiota in immune-related neurological disorders: a review, J. Neuroinflammation 19 (1) (2022) 154, https://doi.org/10.1186/s12974-022-02510-1.
[54] L. Sun, X. Tan, X. Liang, H. Chen, Q. Ou, Q. Wu, L. Wang, Maternal betaine supplementation mitigates maternal high fat diet-induced NAFLD in offspring mice through gut microbiota, Nutrients 15 (2) (2023), https://doi.org/10.3390/nu15020284.
[55] M. Wang, J. Wan, H. Rong, F. He, H. Wang, J. Zhou, W. Zhou, Alterations in gut glutamate metabolism associated with changes in gut microbiota composition in children with autism spectrum disorder, mSystems 4 (1) (2019) 321–339, https://doi.org/10.1128/msystems.00321-18.
[56] R.E. Steinert, M. Sadaghian Sadabad, H.J.M. Harmsen, P. Weber, The prebiotic concept and human health: a changing landscape with riboflavin as a novel prebiotic candidate, Eur. J. Clin. Nutr. 70 (12) (2016) 1348–1353, https://doi.org/10.1038/ejcn.2016.119.
[57] B. Peng, H. Zhao, T.P. Keerthisinghe, Y. Yu, D. Chen, Y. Huang, M. Fang, Gut microbial metabolite p-cresol alters biotransformation of bisphenol A: enzyme competition or gene induction? J. Hazard Mater. 426 (December 2021) (2022) 128093 https://doi.org/10.1016/j.jhazmat.2021.128093.
[58] J.L. Sonnenburg, F. Bäckhed, Diet-microbiota interactions as moderators of human metabolism, Nature 535 (7610) (2016) 56–64, https://doi.org/10.1038/nature18846.
[59] B.K. Trevelline, K.D. Kohl, The gut microbiome influences host diet selection behavior, Proceedings of the National Academy of Sciences of the United States of America 119 (17) (2022) 1–8, https://doi.org/10.1073/pnas.2117537119.